Journal of Magnetism and Magnetic Materials 327 (2013) 167–171

Contents lists available at SciVerse ScienceDirect

Journal of Magnetism and Magnetic Materials

journal homepage: www.elsevier.com/locate/jmmm

Fabrication of $Co_{0.5}Ni_{0.5}Cr_xFe_{2-x}O_4$ materials via sol–gel method and their characterizations

R.H. Kadam [a], A.P. Birajdar [a], Suresh T. Alone [b], Sagar E. Shirsath [c,*]

[a] Materials Research Laboratory, Srikrishna Mahavidyalaya Gunjoti, Omerga, Osmanabad 413613, Maharashtra, India
[b] Department of Physics, RS Art's, Science and Commerce College, Pathri, Aurangabad, Maharashtra, India
[c] Spin Device Technology Center, Department of Information Engineering, Shinshu University, Nagano 380-8553, Japan

ARTICLE INFO

Article history:
Received 30 August 2012
Received in revised form
19 September 2012
Available online 5 October 2012

Keywords:
Ferrite nanoparticle
Cation distribution
Magnetization

ABSTRACT

$Co_{0.5}Ni_{0.5}Cr_xFe_{2-x}O_4$ nanoparticles have been designed by the sol–gel auto combustion method, using nitrates of the respective metal ions, and citric acid as the starting materials. The process takes only a few minutes to obtain as-received Cr-substituted Co–Ni ferrite powders. X-ray diffraction (XRD), vibrational sample magnetometer (VSM), transmission electron microscopy (TEM) are utilized in order to study the effect of variation in the Cr^{3+} substitution and its impact on particle size, lattice constant, specific surface area, cation distribution and magnetic properties. Lattice parameter, particle size found to decrease with increasing Cr^{3+} content, whereas specific surface area showed increasing trend with the Cr^{3+} substitution. Cation distribution indicates that the Cr, Co and Ni ions show preference toward octahedral [B] site, whereas Fe occupies both tetrahedral (A) and octahedral [B] sites. Saturation magnetization (M_S) decreased from 65.1 to 40.6 emu/g with the increase in Cr^{3+} substitution. However, Coercivity increased from 198 to 365 Oe with the Cr^{3+} substitution.

1. Introduction

Nanocrystalline magnetic alloys such as Ni–Cu, Co–Ni, Fe–Co and Fe–Co–Cu are promising candidates for hyperthermia and microwave applications because their magnetic transition temperatures and micro-wave absorbance characteristics vary with composition and grain size [1–5]. As important magnetic materials, Ni–Co alloys have potential application in high-density magnetic recording media, ferrofluids technology, magnetic resonance imaging, high-temperature catalysts, microwave absorber and electromagnetic shielding material [6–9]. Recently, the preparation methods and applications of one-dimensional (1D) Ni–Co alloy materials have been paid more attention due to their unique properties of low dimensionality [10].

Further, Bahgat et al. [11] stated that Ni–Co–Fe alloy has magnetostrictive properties so it can be used for making the magneto-resistance element such as a magneto-resistance sensor, a magneto-resistance head, etc. [12]. Ni–Co–Fe ternary alloys, rich in Co, have been reported with higher saturation magnetic flux density and lower coercivity than $Ni_{80}Fe_{20}$-Permalloy, which can be used to develop more sensitive thin film magnetic heads for high-density recording [13]. In the inverse spinal structure the divalent atoms such as Co^{2+} and Ni^{2+} occupy the octahedral [B] sites, whereas the trivalent atoms Fe^{3+} are equally distributed among the tetrahedral (A) and octahedral [B] sites. $CoFe_2O_4$ and $NiFe_2O_4$ both in their bulk form have inverse spinel structures and the magnetic properties of these ferrites depend on the type of the cations and their distribution among the tetrahedral and octahedral positions [14].

In our previous study we have observed some significant changes in the ferrite materials brought by Cr^{3+} ions [15,16]. Therefore, in the present study we have focused to investigate structural and magnetic properties of Cr^{3+} substituted Ni–Co alloys with the chemical formula $Co_{0.5}Ni_{0.5}Cr_xFe_{2-x}O_4$.

2. Experimental

The powders were synthesized by sol–gel auto-combustion. Analytical grade citric acid ($C_6H_8O_7 \cdot H_2O$), nickel nitrate ($Ni(NO_3)_2 \cdot 6H_2O$), cobalt nitrate ($Co(NO_3)_2 \cdot 3H_2O$), chromium nitrate ($Cr(NO_3)_3 \cdot 9H_2O$) and iron nitrate ($Fe(NO_3)_3 \cdot 9H_2O$) were used as starting materials. Reaction procedure was carried out in air atmosphere without protection of inert gases. The molar ratio of metal nitrates to citric acid was taken as 1:3. The metal nitrates were dissolved together in a minimum amount of double distilled water to get a clear solution. An aqueous solution of citric acid was mixed with metal nitrates solution, then ammonia solution was slowly added to adjust the pH at 7. The mixed solution was kept on to a hot plate with continuous stirring at 90 °C.

* Corresponding author. Tel.: +919421666605; fax: +818048186605.
E-mail address: shirsathsagar@hotmail.com (S.E. Shirsath).

0304-8853/$ - see front matter © 2012 Elsevier B.V. All rights reserved.
http://dx.doi.org/10.1016/j.jmmm.2012.09.059

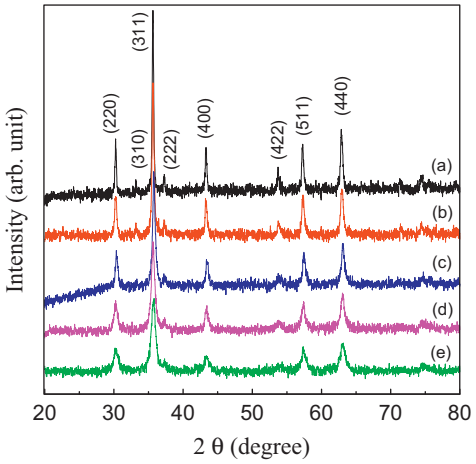

Fig. 1. X-ray diffraction patterns, where (a) $x=0.0$, (b) $x=0.25$, (c) $x=0.50$, (d) $x=0.75$ and (e) $x=1.0$ for $Co_{0.5}Ni_{0.5}Cr_xFe_{2-x}O_4$.

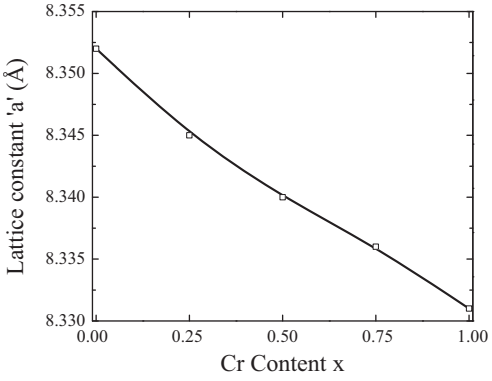

Fig. 2. Variation of lattice constant (a) with Cr content x.

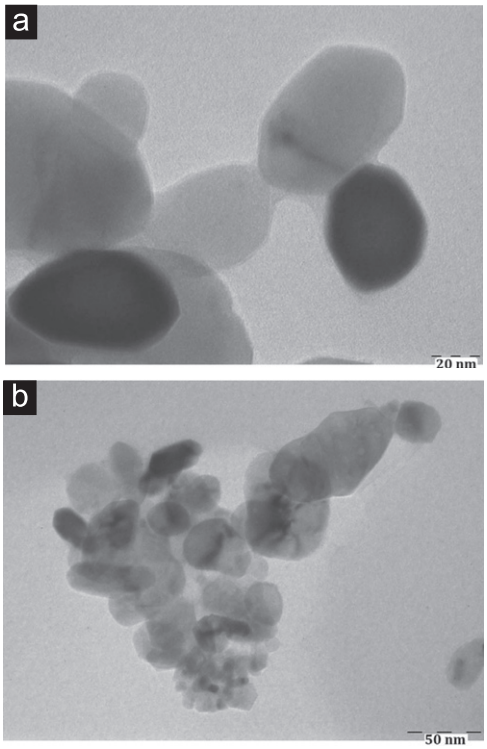

Fig. 3. TEM images of the typical samples (a) $x=0.0$ and (b) $x=1.0$.

During evaporation, the solution became viscous and finally formed a very viscous brown gel. When finally all water molecules were removed from the mixture, the viscous gel began frothing. After few minutes, the gel automatically ignited and burnt with glowing flints. The decomposition reaction would not stop before the whole citrate complex was consumed. The auto-combustion was completed within a minute, yielding the brown-colored ashes termed as a precursor. The as prepared powder then annealed at 600 °C for 4 h. Part of the powder was X-ray examined by Phillips X-ray diffractometer (Model 3710) using Cu-K_α radiation ($\lambda=1.5405$ Å). The magnetic measurements were performed at room temperature using a commercial PARC EG&G VSM 4500 vibrating sample magnetometer. The magnetic hysteresis loops were measured at room temperature with the maximum applied magnetic fields of 0.75 T.

3. Results and discussion

3.1. Structural analysis

Fig. 1 shows the X-ray diffraction (XRD) patterns of all the samples. The XRD patterns exhibit peaks corresponding to the Cr^{3+} substituted Ni–Co ferrites and the absence of any other impurity phases. The results obtained by the X-ray diffraction (XRD) are in good agreement with the JCPDS card (22-1086) and JCPDS card (74-2081). The lattice parameter 'a' was calculated using the following equation [17]:

$$a = d\sqrt{\left(h^2+k^2+l^2\right)} \tag{1}$$

where d is the inter-planer spacing and (hkl) is the index of the XRD reflection peak. It is observed from Fig. 2 that the lattice constant 'a' decreased from 8.352 to 8.331 Å with increase in Cr^{3+} substitution in Ni–Co alloys. The decrease in lattice constant is related to the ionic radii of the respective ions. In the present ferrite system smaller Cr^{3+} of 0.63 Å ionic radii replaces larger Fe^{3+} ions with 0.67 Å ionic radii. Similar variation for Cr^{3+}–Fe^{3+} ions is observed in the literature [18,19].

Transmission electron micrographs (TEM) of the synthesized powder for the typical samples are presented in Fig. 3(a) and (b). It is observed from the TEM images that the particles are slightly agglomerated. The particles are tending to agglomerate because they experience a permanent magnetic moment proportional to their volume. The particle size of the synthesized powder is about 42–27 nm in size and exhibited more or less spherical morphology. In order to confirm of the particle size obtained from the TEM images, we have calculated the crystallite size 'D' of the samples from the most intense (311) peak of XRD and using the Scherrer formula [17],

$$D = \frac{0.9\lambda}{B\cos\theta} \tag{2}$$

where λ is the wavelength used in XRD, B is the full width at half maximum in radian (2θ), θ is the corresponding Bragg angle. The crystallite size of each sample obtained in this way is displayed in Fig. 4. The crystallite size decreased from 36 to 24 nm with the increase in Cr^{3+} substitution. The difference of particle size values obtained by XRD and TEM methods may be attributed to the presence of amorphous region inside the grain itself [20].

The specific surface area (S) was calculated from the diameter of the particle in nanometers and the measured density using the following relation [21]:

$$S = 6000/Dd_B \tag{3}$$